ELSEVIER

Journal of Quantitative Spectroscopy & Radiative Transfer 103 (2007) 601–610

Journal of Quantitative Spectroscopy & Radiative Transfer

www.elsevier.com/locate/jqsrt

A diffusion-based approximate model for radiation heat transfer in a solar thermochemical reactor

L.A. Dombrovsky[a,*], W. Lipiński[b], A. Steinfeld[b,c]

[a]*Institute for High Temperatures of the Russian Academy of Sciences, Krasnokazarmennaya 17A, 111116, Moscow, Russia*
[b]*Department of Mechanical and Process Engineering, ETH Zurich, Sonnegstrasse 3, 8092 Zurich, Switzerland*
[c]*Solar Process Technology, Paul Scherrer Institute, 5232 Villigen, Switzerland*

Received 9 May 2006; received in revised form 2 August 2006; accepted 9 August 2006

Abstract

An approximate numerical method for fast calculations of the radiation heat transfer in a solar thermochemical reactor cavity is formulated based on the separate treatment of the solar and thermal radiative exchange by the diffusion approach. The usual P_1 approximation is generalized by applying an equivalent radiation diffusion coefficient for the optically thin central part of the cavity. The resulting boundary-value problems are solved using the finite element algorithm. The accuracy of the model is assessed by comparing the results to those obtained by a pathlength-based Monte Carlo simulation. The applicability of the proposed model is demonstrated by performing calculations for an example problem, which incorporates a range of parameters typical for a solar chemical reactor and the spectral radiative properties of polydisperse zinc oxide particles.
© 2006 Elsevier Ltd. All rights reserved.

Keywords: Radiation; Diffusion approximation; Monte Carlo; Zinc oxide; Solar energy

1. Introduction

Solar thermochemical processing makes use of concentrated solar radiation as the energy source of high-temperature heat for driving endothermic reactions [1]. It offers several advantages over the combustion-based technology. Energy is efficiently transferred via direct irradiation to the reaction site, bypassing the limitations imposed by indirect heat transfer through heat exchangers in external combustion, or eliminating the quality degradation of chemical products by combustion gases and soot in internal combustion. The emission of greenhouse gases is avoided, and in the case of the fuel production or upgrade, the final product contains chemically stored solar energy. Example applications include the thermal decomposition of limestone, the thermal reduction of metal oxides, the thermal cracking/reforming of natural gas, and the thermal gasification of coal. In particular, solar high-flux irradiation is used for the thermal dissociation of zinc oxide

$$2\mathrm{ZnO(s)} \rightarrow 2\mathrm{Zn(g)} + \mathrm{O_2(g)} \tag{1}$$

*Corresponding author. Tel.: +7 495 362 5590/250 3264; fax: +7 495 362 5590.
E-mail address: dombr@online.ru (L.A. Dombrovsky).

0022-4073/$ - see front matter © 2006 Elsevier Ltd. All rights reserved.
doi:10.1016/j.jqsrt.2006.08.003

at temperatures above 2100 K [2]. The importance of this reaction relies in the variety of applications of Zn as an energy carrier, e.g., its hydrolysis for hydrogen production as part of a 2-step water splitting cycle. The solar reactor features a rotating cavity-receiver lined with micron-size ZnO particles that are directly irradiated and dissociated. A complete description of the combined heat transfer in the reactor includes the complex spectral description of thermal radiation by walls and particles and of the incoming solar flux, and by accounting for varying particle concentration within the cavity-receiver.

Previous pertinent studies of radiative heat transfer within particle suspensions exposed to concentrated solar radiation include steady-state models based on the discrete ordinates method [3], on the six-flux method [4], and on the Monte Carlo (MC) method [5]. Radiative heat transfer analysis in participating media undergoing thermochemical transformation under direct irradiation was performed by a steady-state model based on MC [6], and by transient models based on the Rosseland approximation [7,8] and on MC [9]. Iterative or transient computations employing the general MC technique require time-consuming full ray-tracing runs for each iteration or time step.

This paper presents an approximate numerical method for fast calculations of the radiative heat transfer in a solar thermochemical reactor cavity containing ZnO particles of spatially varying size and concentration. The method is based on the diffusion approach (DA) [10,11]. The accuracy of the model is assessed by comparing the results to those obtained by a pathlength-based MC simulation [12]. The applicability of the proposed model is demonstrated by performing calculations for the model reaction (1), which incorporates a range of parameters typical for a solar chemical reactor and spectral radiative properties of ZnO particles.

2. Problem statement

A solar thermochemical reactor for the thermal dissociation of semi-transparent ZnO particles under concentrated solar irradiation is considered [13]. The reactor features a rotating cylindrical cavity with a windowed aperture at its front wall. ZnO particles are supplied by the axial feeding system, operating cyclically. The small particles fall irregularly by gravity and inertial forces to the lateral wall while being heated and decomposed into the gaseous products Zn and O_2. The geometry of the model problem is depicted in Fig. 1. Three axisymmetric regions within the cavity are distinguished: (1) the non-participating empty central part; (2) the particle cloud of small ZnO particles; and (3) the particle bed at the lateral wall.

The particle average radius $a_{32} = 10\,\mu m$ and volume fraction $f_v = 10^{-3}$ are assumed in the cloud and $a_{32} = 500\,\mu m$, $f_v = 10^{-1}$ are assumed in the particle bed. The value a_{32} is defined as follows:

$$a_{32} = \int_0^\infty a^3 F(a)\mathrm{d}a \Big/ \int_0^\infty a^2 F(a)\mathrm{d}a, \tag{2}$$

where $F(a)$ is the size distribution function.

The cavity walls are assumed to be gray and diffuse with hemispherical emissivity of $\varepsilon_w = 0.8$ and at uniform temperature 1600 K. The incoming integral solar flux $q''_{in} = 2.5\,MW/m^2$ is assumed diffuse and

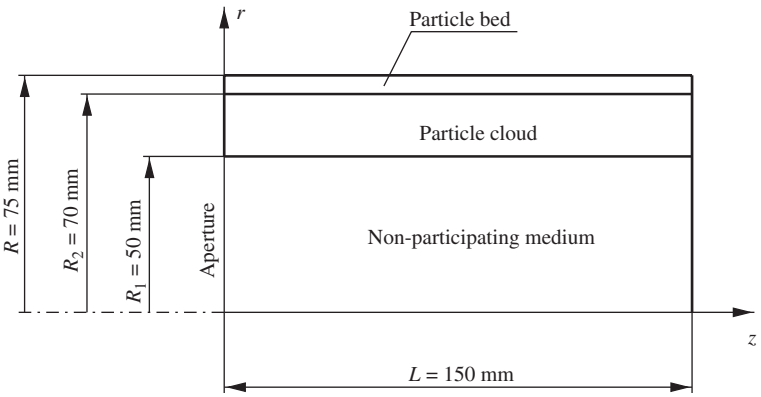

Fig. 1. Scheme of a thermochemical reactor cavity.

uniformly distributed over the aperture, but the model can be extended to include directional and non-uniform distributions of the incident solar radiation. Its spectral distribution is approximated by that of a blackbody at $T_{in} = 5780\,K$. The particle temperature in the cloud is assumed constant and equal to 2200 K. In the particle bed, we assume a linear radial dependence of particle temperature from 2000 K to the wall temperature.

3. Radiative properties

Radiative properties of the participating medium within the cavity are derived by neglecting the radiation absorption by gaseous phase, consisting of O_2, Zn and Ar at atmospheric pressure. The particle radiative properties are evaluated using the optical constants of ZnO, the local particle volume fraction f_v, and the particle size distribution $F(a)$. The index of refraction is assumed constant $n_\lambda = 1.9$. The index of absorption is obtained by approximating the data from [15] as

$$k_\lambda = \begin{cases} k_0, & \lambda < \lambda_1, \\ (k_0 - k_1)/[1 + \gamma(\lambda^2 - \lambda_1^2)] + k_1, & \lambda > \lambda_1, \end{cases} \tag{3}$$

where $k_0 = 0.5$, $\lambda_1 = 0.37\,\mu m$, $\gamma = 120\,\mu m^{-2}$ and $k_1 = 10^{-4}$.

Variation of the absorption index with the parameter k_1 is shown in Fig. 2. Also plotted are the values obtained from the theoretical model [15]. While the refractive index is widely available in the literature [15–18], the infrared absorption index of ZnO is not reported, and relation (3) is assumed for the range $\lambda > 0.8\,\mu m$. Since the long-wave index of absorption strongly varies with the parameter k_1, this assumption may lead to a significant error in the infrared absorption and emission by particles.

The transport approximation of the scattering phase function is employed, simplifying the formulation of a radiative transfer problem. As a result, only the efficiency factor of absorption and the transport efficiency factor of extinction are required. This approach is known to be sufficiently accurate for radiative transfer calculations in numerous applications [10,11].

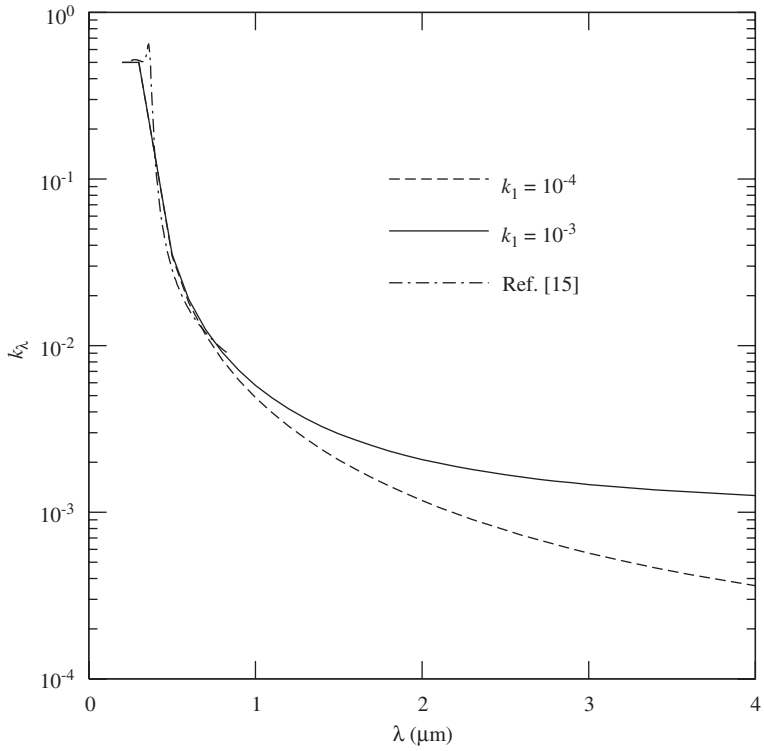

Fig. 2. Index of absorption of zinc oxide.

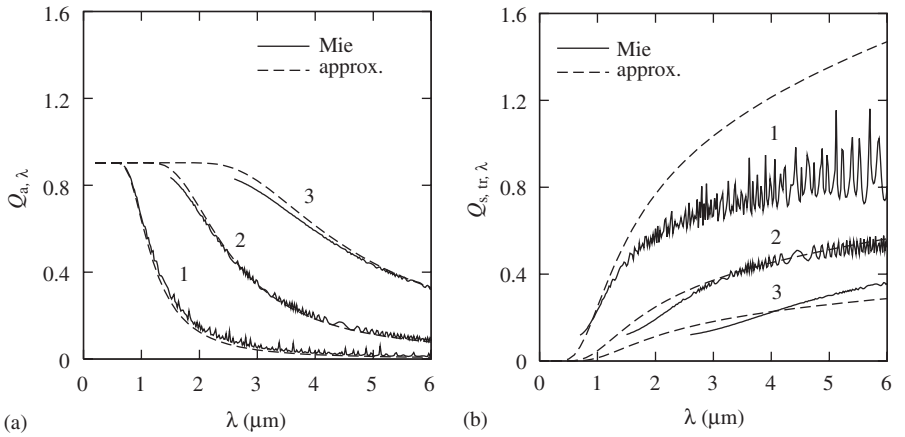

Fig. 3. Radiative characteristics of ZnO particles for particle radii a (1) 10, (2) 100 and (3) 500 μm, calculated by using approximation (4), and by the Mie theory: (a) absorption efficiency factor; (b) transport scattering efficiency factor.

The efficiency factors for absorption, transport scattering, and transport extinction of a single weakly absorbing particle are calculated as [14]

$$Q_{a,\lambda}=\frac{4n_\lambda}{(n_\lambda+1)^2}[1-\exp(-4k_\lambda x)],\quad Q_{s,tr,\lambda}=\begin{cases} C\zeta, & \zeta\leqslant 1\\ C/\zeta^\gamma, & \zeta>1\end{cases},\quad Q_{ext,tr,\lambda}=Q_{a,\lambda}+Q_{s,tr,\lambda}, \tag{4}$$

where $C=1.5n_\lambda(n_\lambda-1)\exp(-15k_\lambda)$, $\gamma=1.4-\exp(-80k_\lambda)$, $\zeta=0.4(n_\lambda-1)x$ and $x=2\pi a/\lambda$. The absorption and transport scattering efficiency factors of ZnO particles for particle radii $a=10$, 100 and 500 μm and $k_1=10^{-4}$ are shown in Figs. 3a and b, respectively. Also plotted are curves for the efficiency factors obtained from the Mie theory. The approximation of the absorption efficiency factor is accurate for both small and large particles over the whole spectral range. In contrast, the agreement between the approximated and Mie transport efficiency factors of scattering is good for large particles but the approximation overestimates the scattering by small particles in the long-wave range. The latter error is expected to have minor impact on the radiative transfer in the example problem due to negligible role of the long-wave radiation scattering by a particle cloud.

Absorption, transport scattering and transport extinction coefficients of polydisperse particles are obtained from [10]

$$\{\kappa_\lambda,\sigma_{s,tr,\lambda},\beta_{tr,\lambda}\}=0.75f_v\int_0^\infty\{Q_{a,\lambda},Q_{s,tr,\lambda},Q_{ext,tr,\lambda}\}a^2F(a)\,da\Big/\int_0^\infty a^3F(a)\,da, \tag{5}$$

where f_v is the particle volume fraction. In the monodisperse approximation based on the average particle radius a_{32}, the absorption, scattering and extinction coefficients are given by

$$\{\kappa_\lambda,\sigma_{s,tr,\lambda},\beta_{tr,\lambda}\}=0.75f_v\{Q_{a,\lambda},Q_{s,tr,\lambda},Q_{ext,tr,\lambda}\}/a_{32}, \tag{6}$$

where the efficiency factors are determined for $a=a_{32}$.

Figs. 4a and b show the spectral absorption and scattering coefficients of ZnO particles for $k_1=10^{-4}$, respectively. The curves obtained in the monodisperse approximation agree well with those for the selected polydisperse systems ($F(a)\sim\exp[-(a-a_m)^2/(2\sigma^2)]$) for both $a_{32}=10$ and 500 μm in the considered spectral region. Therefore, the monodisperse approximation is selected for further analysis.

4. Reference MC solution

The pathlength MC with ray redirection is applied to solve for the radiative exchange in the cavity [12]. The method is known to produce sufficiently accurate results for a large enough number of stochastic rays while

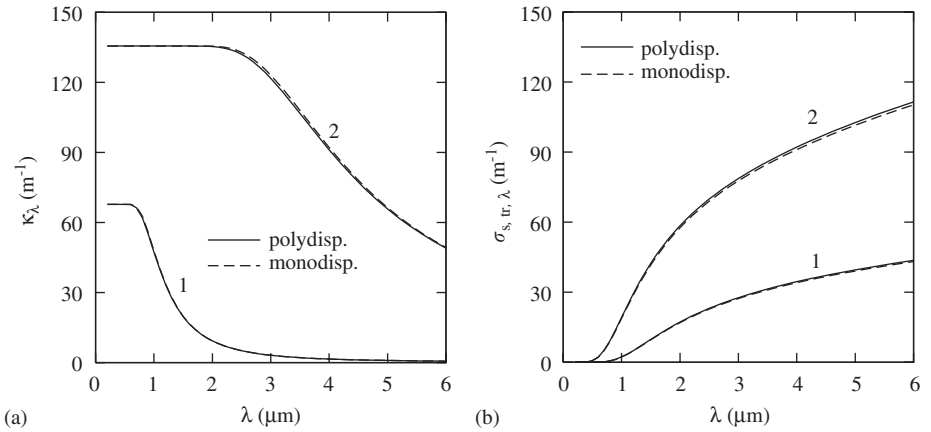

Fig. 4. Absorption (a) and transport scattering (b) coefficients: (1) $a_{32} = 10$, (2) 500 μm.

the computational time requirements are smaller than those for the collision-based MC. The net radiative flux to a wall element dA and the divergence of the radiative flux within an elementary volume dV of the participating medium are calculated as

$$q''_{r,w} = \frac{d\left(\sum_{k_w} \varepsilon_w q_{ray,k_w}\right)}{dA_w} - \varepsilon_w \sigma T_w^4, \tag{7}$$

$$\nabla q''_{r,p} = 4\kappa_{P,p}\sigma T_p^4 - \frac{\sum_{k_p} q_{ray,k_p} \kappa_{\lambda,p} dl_{k_p}}{dV_p}, \tag{8}$$

where k_w and k_p designate rays reflected by the wall element dA_w and traversing the medium volume dV_p, respectively. q_{ray,k_p} represents the power of the k_p'th ray entering volume dV_p, and dl_{k_p} is the path length of k_p'th ray within dV_p. The MC code employs the probability density functions for the azimuthal and polar angles φ and θ, and the wavelength λ for emission/scattering by the non-gray medium, and for emission/reflection by gray-diffuse walls [11,12]. Isotropic scattering is assumed for conforming the MC procedure to the transport approximation. The finite volume technique is applied to obtain the discrete forms of Eqs. (7) and (8) on the structured cylindrical grid of $30 \times 3 \times 30$ elements.

5. Diffusion approximation

In the diffusion approximation, the spectral radiative flux is adopted in the following form [10]:

$$q''_{r,\lambda} = -D_\lambda \nabla G_\lambda, \quad G_\lambda = \int_0^{4\pi} I_\lambda \, d\Omega, \tag{9}$$

where D_λ is the radiation diffusion coefficient, proportional to the mean free path of radiation. Substituting Eq. (9) into the direction-integrated equation of radiative transfer leads to the boundary-value problem for the direction-integrated spectral radiative intensity G_λ [10]. In the DA presented here, radiation heat losses from the cavity are determined mainly by thermal radiation of particles and walls, whereas the contribution of the scattered solar radiation is neglected. This enables one to split the solution into two steps. In the first step, the radiative exchange in the cavity is solved for the thermal radiation emitted by the walls and particles with the inclusion of the central (non-participating) part of the medium region while omitting solar radiation. The corresponding boundary-value problem is formulated as follows:

$$-\nabla(D_\lambda \nabla G_\lambda) + \kappa_\lambda G_\lambda = \kappa_\lambda 4\pi I_{b\lambda}(T_p), \tag{10}$$

$$-D_\lambda \hat{n}_w \cdot \nabla G_{\lambda,w} = \delta\gamma_w [G_{\lambda,w} - S_{\lambda,w}], \tag{11}$$

$$\delta = \begin{cases} 0 & \text{for } r = 0, \\ 1 & \text{elsewhere at boundaries,} \end{cases} \tag{12}$$

$$S_{\lambda,\mathrm{w}} = \begin{cases} 0 & \text{for } z = 0 \text{ and } 0 \leqslant r < R_1, \\ 4\pi I_{\mathrm{b}\lambda}(T_{\mathrm{w}}) & \text{elsewhere at boundaries,} \end{cases} \tag{13}$$

where $\gamma_{\mathrm{w}} = 0.5\varepsilon_{\mathrm{w}}/(2-\varepsilon_{\mathrm{w}})$ and $\hat{n}_{\mathrm{w}}$ is the normal vector pointing into the boundary. The usual form of the diffusion coefficient $D_\lambda = 1/(3\beta_{\mathrm{tr},\lambda})$, which corresponds to the P_1 approximation [10,11], is used for the particulate medium. However, the medium in the central part of the computational region ($r < R_1$) is not participating and this relation cannot be used for $\beta_{\mathrm{tr},\lambda} = 0$. Instead, a constant value of the radiation diffusion coefficient $D_\lambda = 2R_1H/(2R_1 + H)$ is employed for $r < R_1$ by recalling the physical meaning of D_λ. The model calculations showed that the results are not sensitive to the choice of this expression.

In the second step of the solution, the reflection of solar radiation from the particle cloud and from the central part of the back wall is neglected. Hence, the spectral solar radiation fluxes to the cloud and to the central part of the back wall are given by [11]

$$q''_{\lambda,\mathrm{c}} = \frac{q''_{\mathrm{in}}}{\sigma T_{\mathrm{s}}^4}\,\pi I_{\lambda\mathrm{b}}(T_{\mathrm{s}})\left(\frac{Z^2+0.5}{\sqrt{Z^2+1}} - Z\right), \quad Z = z/(2R_1), \tag{14}$$

$$q''_{\lambda,\mathrm{w,back}} = 0.5\,\frac{q''_{\mathrm{in}}}{\sigma T_{\mathrm{s}}^4}\,\pi I_{\lambda\mathrm{b}}(T_{\mathrm{s}})\varepsilon_{\mathrm{w}}\left(X - \sqrt{X^2-4}\right), \quad X = 2 + (L/R_1)^2. \tag{15}$$

Note that Eqs. (14) and (15) are valid only for the diffuse and uniform incident solar flux. In a more general case, the fluxes to the cloud and to the central part of the back wall can be obtained by using MC. The boundary-value problem for the second step reduces to the computational region including the particle cloud and the bed only. The thermal radiation from particles and walls is omitted, but the incoming solar flux is included in the boundary condition at the cloud surface. This is formulated as

$$-\nabla(D_\lambda \nabla G_\lambda) + \kappa_\lambda G_\lambda = 0, \tag{16}$$

$$-D_\lambda \hat{n}_{\mathrm{w}} \cdot \nabla G_{\lambda,\mathrm{w}} = \gamma_{\mathrm{w}}[G_{\lambda,\mathrm{w}} - S_{\lambda,\mathrm{w}}], \tag{17}$$

$$S_{\lambda,\mathrm{w}} = \begin{cases} 4q''_{\lambda,\mathrm{c}} & \text{for } 0 \leqslant z < L \text{ and } r = R_1, \\ 0 & \text{at the cavity walls.} \end{cases} \tag{18}$$

Due to the linearity of the problem, the final solution including radiative flux and its divergence is obtained as a sum of the solutions for the two steps.

The boundary-value problems (10)–(13) and (16)–(18) are solved by the finite element method on the structured grid consisting of $40 \times 40 \times 2$ circular elements of triangular cross section [10].

6. Results

Numerical computations were performed for the model problem using both MC and DA. Fig. 5 shows the integral radiative heat flux to the front (including the aperture) and back walls of the cavity. The agreement between the MC and DA is better for the back wall than for the front wall. The MC and DA profiles converge at $r/R \to 1$.

Axial profiles of the radiative fluxes are shown in Fig. 6. The best agreement between the MC and DA results is achieved at the lateral wall, where the profiles are almost identical. In contrast, the maximum differences are found at the cloud boundary.

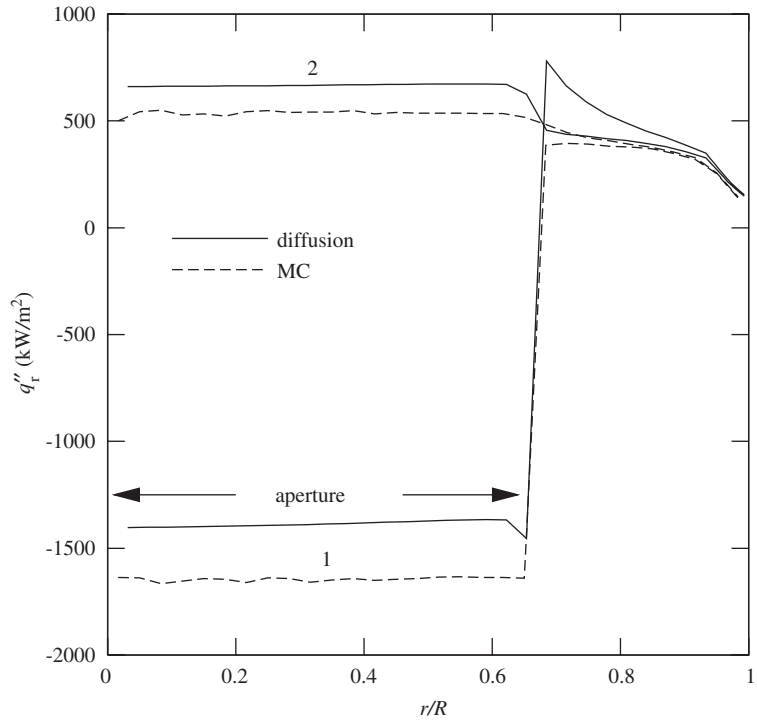

Fig. 5. Radial profiles of net radiative flux to (1) front wall (including aperture) and (2) back wall.

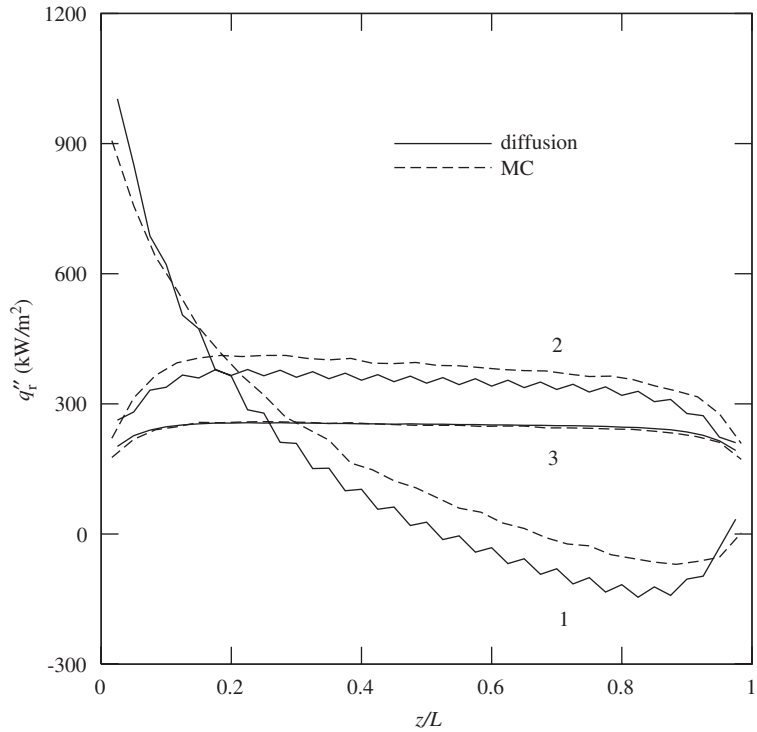

Fig. 6. Axial profiles of net radiative flux to (1) cloud, (2) cloud-bed interface, and (3) lateral wall.

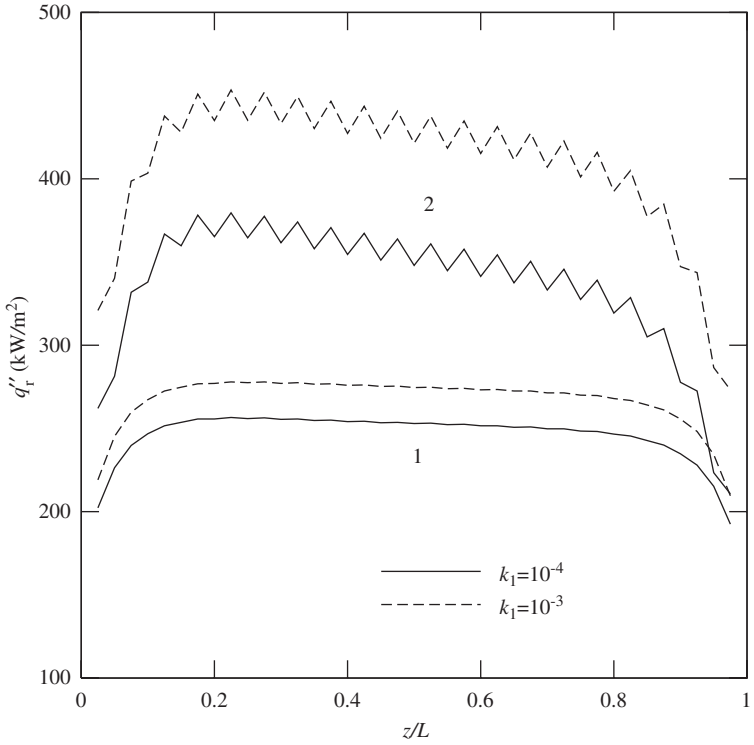

Fig. 7. Axial profiles of net radiative flux to (1) cloud-bed interface, and (2) lateral wall.

The source of errors of the DA method was examined by performing additional calculations for a case with the solar flux set to zero. It was found that the overestimation of the axial radiative fluxes to the front and back walls is a consequence of the overestimated fluxes in the first step of the solution, i.e., when the only source of radiation is the emission by walls and particles. The overestimation at the aperture is bigger for the case with the solar flux set to zero than that for the reference case with solar radiation included, because the solar radiation reflected and scattered towards the aperture is neglected in the DA method but included in the MC method. The radial radiative flux resulting from the incoming solar radiation is modeled properly by DA at selected locations for both the reference case and the case with no solar flux.

The quality of both MC and DA results increases with increasing r/R ratio. While this effect is explained for MC by decreasing size of the control elements with decreasing radius, it is caused by the FEM discretisation in the DA approach. The selected resolution of the unstructured triangular grid in the DA method also leads to oscillations in the curves shown in Figs. 5–7. The accuracy of the MC results was determined by calculating the $P = 95\%$ confidence intervals $\bar{\varphi} \pm t_{\nu,P\%} S_\varphi / \sqrt{n_{MC}}$ for $\nu = n_{MC} - 1 = 9$ degrees of freedom. The absolute confidence interval for the radiative flux was maximum at the aperture ($r/R = 0.0167$, $q''_{r,w} = -1636.2 \pm 63.5\,\mathrm{kW/m^2}$), whereas for its divergence it was maximum for the bed ($r/R = 0.95$, $z/L = 0.25$, $\nabla \cdot q''_r = 6776.5 \pm 1835.1\,\mathrm{kW/m^3}$).

A typical MC simulation was performed for the total number of rays $n_{ray} = 10^7$ and took about 5000 s on a PC with a Pentium 4 3.2 GHz processor. In contrast, a typical DA simulation lasted less than 3 s. The short computational time makes the DA method attractive for solving transient combined heat transfer problems.

The DA model, including the approximations for the radiative characteristics of particles, is convenient for studying the effect of particle parameters on radiation heat transfer in the solar thermochemical reactor. For example, the role of the infrared absorption index of ZnO is illustrated in Fig. 7. Interestingly, radiation absorption in the particle bed is approximately 50% greater in the case of $k_1 = 10^{-3}$ than that in the baseline variant with $k_1 = 10^{-4}$. This high sensitivity of the results to the infrared absorption index of ZnO indicates the importance of its experimental validation.

7. Conclusions

An approximate numerical method based on the DA for fast calculations of the radiation heat transfer in a solar thermochemical reactor cavity is presented. The method comprises separate calculations for the incoming solar flux and thermal radiation emitted by the particles and cavity walls. The calculations are based on P_1 approximation and the finite element method, and have been performed for a medium with a realistic strong radial variation of the radiative properties due to the varying particle concentration and diameter. The numerical validation of the diffusion approximation method by the reference MC technique shows a good agreement of the results, in particular for the radial radiative flux. At the same time, the MC simulation is recommended for an intermediate control of the DA results for typical ranges of the problem parameters.

An approximate form of the absorption and transport scattering efficiency factors for semitransparent ZnO particles is used. The approximations are validated by comparing them with the exact values obtained from the Mie theory. A comparison of radiation coefficients for the mono- and polydisperse medium indicates that monodisperse approximation can be employed without detrimental effects. The approximate relations for the main absorption and scattering characteristics of particles and the monodisperse approximation lead to additional significant simplification of the calculations.

The simplified model for radiative properties and radiation heat transfer enables a significant reduction of the computational time in calculations for combined transient heat transfer problems requiring the calculation of the radiation field at each time step of numerical solution. Furthermore, it makes possible the implementation of the complete spectral radiation transfer calculations in problem-oriented CFD codes for the complex analysis of the solar thermochemical reactors.

The parameter study performed by using the approximate model indicated the importance of the experimental determination of the ZnO near-infrared absorption spectrum for an accurate simulation of the radiative exchange in the particle cloud.

Acknowledgments

This work was partially supported by Russian Foundation of Basic Research (Grant no. 04-02-16014) and BFE—Swiss Federal Office of Energy. We thank R. Müller for the information on the solar thermochemical reactor and particle characteristics, and J. Howell for the consultation on the pathlength MC technique.

References

[1] Steinfeld A, Palumbo R. Solar thermochemical process technology. In: Meyers RA, editor. Encyclopedia of physical sciences and technology, vol. 15. San Diego: Academic Press; 2003. p. 237–56.
[2] Steinfeld A. Solar hydrogen production via a 2-step water-splitting thermochemical cycle based on Zn/ZnO redox reactions. Int J Hydrogen Energy 2002;27:611–9.
[3] Evans G, Houf H, Greif R, Crowe C. Gas-particle flow within a high temperature solar cavity receiver including radiation heat transfer. J Sol Energy Eng 1987;109:134–42.
[4] Miller F, Koenigsdorff R. Theoretical analysis of a high-temperature small-particle solar receiver. Sol Energy Mater 1991;24:210–21.
[5] Mischler D, Steinfeld A. Nonisothermal nongray absorbing–emitting–scattering suspension of Fe_3O_4 particles under concentrated solar irradiation. J Heat Transfer 1995;117:346–54.
[6] Hirsch D, Steinfeld A. Radiative transfer in a solar chemical reactor for the co-production of hydrogen by thermal decomposition of methane. Chem Eng Sci 2004;59:5771–8.
[7] Lipiński W, Steinfeld A. Heterogeneous decomposition under direct irradiation. Int J Heat Mass Transfer 2004;47:1907–16.
[8] Osinga T, Olalde G, Steinfeld A. The solar carbothermal reduction of ZnO—Shrinking packed-bed reactor modeling and experimental validation. Ind Eng Chem Res 2004;43:7981–8.
[9] Lipiński W, Z'Graggen A, Steinfeld A. Transient radiation heat transfer within a non-gray non-isothermal absorbing–emitting–scattering suspension of reacting particles undergoing shrinking. Numer Heat Transfer, Part B 2005;47:443–57.
[10] Dombrovsky LA. Radiation heat transfer in disperse systems. New York: Begell House; 1996.
[11] Modest MF. Radiative heat transfer. San Diego: Academic Press; 2003.
[12] Farmer JT, Howell JR. Comparison of Monte Carlo strategies for radiative transfer in participating media. Adv Heat Transfer 1998;31:333–429.

[13] Müller R, Häberling P, Palumbo RD. Reactor for direct utilization of external radiation heat for thermal or thermo-chemical material processes. European patent no. 04 026 418.6, 2004.
[14] Dombrovsky LA. A spectral model of absorption and scattering of thermal radiation by diesel fuel droplets. High Temp 2002;40:242–8.
[15] Yoshikawa H, Adachi S. Optical constants of ZnO. Jpn J Appl Phys 1997;36:6237–43.
[16] Ghosh G. Handbook of thermo-optic coefficients of optical materials with applications. San Diego: Academic Press; 1998.
[17] Bond WL. Measurement of refractive indices of several crystals. J Appl Phys 1965;36:1674–7.
[18] Park YS, Schneider JR. Index of refraction of ZnO. J Appl Phys 1968;39:3049–52.